A USP28–53BP1–p53–p21 signaling axis arrests growth after centrosome loss or prolonged mitosis

Bramwell G. Lambrus,[1]* Vikas Daggubati,[1]* Yumi Uetake,[2] Phillip M. Scott,[1] Kevin M. Clutario,[1] Greenfield Sluder,[2] and Andrew J. Holland[1]

[1]Department of Molecular Biology and Genetics, Johns Hopkins University School of Medicine, Baltimore, MD 21205
[2]Department of Cell and Developmental Biology, University of Massachusetts Medical School, Worcester, MA 01655

Precise regulation of centrosome number is critical for accurate chromosome segregation and the maintenance of genomic integrity. In nontransformed cells, centrosome loss triggers a p53-dependent surveillance pathway that protects against genome instability by blocking cell growth. However, the mechanism by which p53 is activated in response to centrosome loss remains unknown. Here, we have used genome-wide CRISPR/Cas9 knockout screens to identify a USP28–53BP1–p53–p21 signaling axis at the core of the centrosome surveillance pathway. We show that USP28 and 53BP1 act to stabilize p53 after centrosome loss and demonstrate this function to be independent of their previously characterized role in the DNA damage response. Surprisingly, the USP28–53BP1–p53–p21 signaling pathway is also required to arrest cell growth after a prolonged prometaphase. We therefore propose that centrosome loss or a prolonged mitosis activate a common signaling pathway that acts to prevent the growth of cells that have an increased propensity for mitotic errors.

Introduction

The centrosome plays a fundamental role in most microtubule-related functions, including cell motility, intracellular transport, and chromosome segregation (Gönczy, 2012; Conduit et al., 2015). Centrosomes have at their core a pair of centrioles that duplicate once per cell cycle to allow a single interphase centrosome to reproduce once before mitosis (Tsou and Stearns, 2006). The two centrosomes then separate and form the poles of the bipolar spindle apparatus upon which chromosomes are segregated. Errors in centriole duplication can lead to an abnormal centrosome number, which disrupts the fidelity of cell division and leads to the production of aneuploid progeny (Ganem et al., 2009; Silkworth et al., 2009).

Polo-like kinase 4 (Plk4) is the conserved, master regulator of centriole copy number (Bettencourt-Dias et al., 2005; Habedanck et al., 2005). In nontransformed human cells, inhibition of Plk4 kinase activity or induced degradation of Plk4 leads to centrosome loss and a p53-dependent cell cycle arrest within a few cell divisions (Lambrus et al., 2015; Wong et al., 2015). This arrest is not caused by mitotic errors, Hippo pathway activation, p38-mediated stress signaling, or DNA damage (Lambrus et al., 2015; Wong et al., 2015). Genetic inactivation of the centriole protein SAS4 in the mouse embryo or in the developing mouse brain also results in centrosome loss, delayed spindle assembly, and p53-dependent apoptosis (Bazzi and Anderson, 2014; Insolera et al., 2014). Together, these studies implicate the existence of a new signaling pathway that activates p53 in response to a signal linked to centrosome loss. For simplicity, we hereafter refer to this pathway as the centrosome surveillance pathway.

Although centrosomes are required for the sustained proliferation of nontransformed mammalian cells, a wide array of tumor cells are able to continue to proliferate after centrosome loss (Wong et al., 2015). Cell divisions that lack centrosomes are error prone (Khodjakov and Rieder, 2001; Debec et al., 2010; Sir et al., 2013; Lambrus et al., 2015), suggesting that the centrosome surveillance pathway could protect against genome instability by preventing the growth of cells with too few centrosomes. Nevertheless, it remains unclear how p53 is activated in response to centrosome loss in mammalian cells. Here, we explore the genetic basis for signaling through the centrosome surveillance pathway.

Results and discussion

A chemical genetic system to activate the centrosome surveillance pathway

We set out to develop a chemical genetic system to specifically inhibit Plk4 kinase activity and induce centrosome loss in human cells. Mutation of a single amino acid in the ATP-binding

*B.G. Lambrus and V. Daggubati contributed equally to this paper.

Correspondence to Andrew J. Holland: aholland@jhmi.edu

Abbreviations used in this paper: AS, analogue sensitive; CMV, cytomegalovirus; sgRNA, single guide RNA.

The Rockefeller University Press $30.00
J. Cell Biol. Vol. 214 No. 2 143–153
www.jcb.org/cgi/doi/10.1083/jcb.201604054

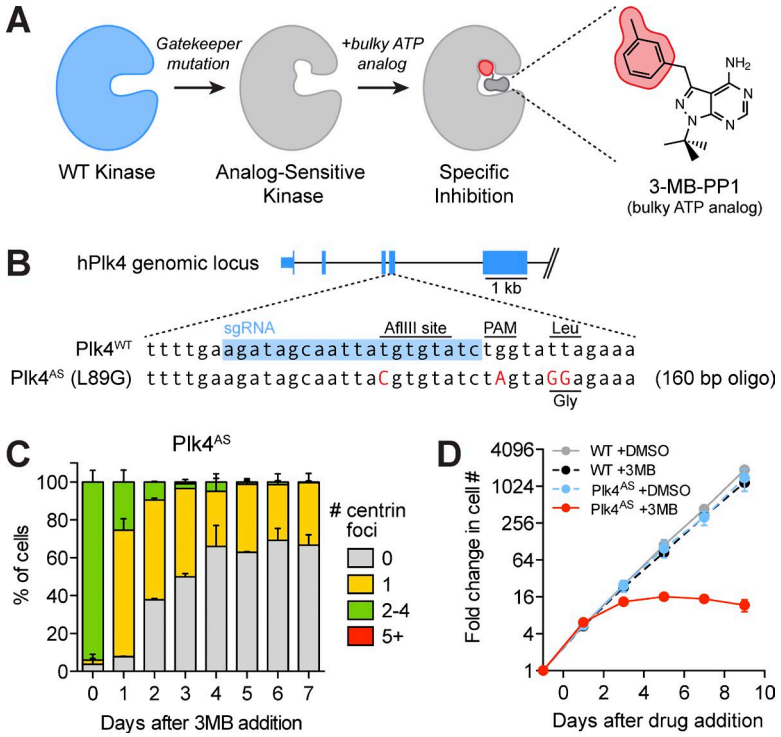

Figure 1. **Inhibition of AS Plk4 leads to centrosome loss and growth arrest.** (A) Principle of AS Plk4 and its inhibition by 3MB-PP1. (B) Schematic of sgRNA and repair template oligo used to knock in the AS mutation at endogenous Plk4 genomic loci. sgRNA sequence is highlighted in blue, and edited nucleotides are displayed in red. (C) Centriole number distribution in interphase Plk4^{AS} cells at time points after addition of 3MB-PP1. Data are means ± SEM of three independent experiments (n = 3) with >80 cells per experiment. (D) Fold increase in cell number after 3MB-PP1 addition. Data are means ± SEM (n = 2, performed in triplicate). WT, wild type.

pocket of Plk4 creates an analogue-sensitive (AS) kinase that can be inhibited with nonhydrolyzable, bulky ATP analogues (Fig. 1 A; Holland et al., 2010; Moyer et al., 2015). We used CRISPR/Cas9 to knock in the Plk4 AS mutation (L89G) into the endogenous Plk4 locus in nontransformed hTERT-RPE1 cells (Fig. 1 B). A clone was identified carrying a frameshift, knockout mutation in one Plk4 allele and an AS knockin mutation in the second allele. The Plk4$^{AS/-}$ cells (hereafter referred to as Plk4^{AS}) proliferated at the same rate as the parental cells and contained normal numbers of centrioles (Fig. 1, C and D). As expected, inhibition of Plk4 kinase activity with 3MB-PP1 led to an increase in Plk4 levels at the centrosome and a failure of centriole duplication (Fig. S1 A and Fig. 1 C).

Although RPE1 cells proliferated normally in the presence of 3MB-PP1, addition of 3MB-PP1 to Plk4^{AS} cells resulted in a penetrant G1 cell cycle arrest after 3 d (Figs. 1 D and S1 B). As a consequence, centriole loss ceased after 4 d of treatment with 3MB-PP1 (Fig. 1 C). To evaluate the long-term growth potential of cells that lack Plk4 kinase activity, we performed clonogenic survival assays. 3MB-PP1 addition prevented colony formation in Plk4^{AS} RPE1 cells but did not affect the survival of parental RPE1 cells (Fig. S1 C). The arrest was not caused by oxidative stress, as growth in low oxygen (3% O_2) did not allow continued growth after centrosome loss (Fig. S1 D). A similar growth arrest was previously reported in RPE1 cells that lose centrosomes as a result of destruction of endogenous Plk4 or treatment with the ATP-competitive Plk4 inhibitor centrinone (Lambrus et al., 2015; Wong et al., 2015). We conclude that inhibition of Plk4^{AS} kinase activity provides a system to activate the centrosome surveillance pathway in RPE1 cells.

Genome-scale CRISPR/Cas9 knockout screen to identify components of the centrosome surveillance pathway

To identify novel components of the centrosome surveillance pathway, we used Plk4^{AS} RPE1 cells to perform a genome-wide, loss-of-function CRISPR/Cas9 screen. We generated Plk4^{AS} cells stably expressing the SpCas9 endonuclease and transduced them with a genome-wide single guide RNA (sgRNA) library (Shalem et al., 2014). Knockout libraries of RPE1 Plk4^{AS} cells were cultured in the presence of DMSO or 3MB-PP1 for 42 d. Cells that lacked genes required for the centrosome surveillance pathway were expected to proliferate in the absence of Plk4 kinase activity and enrich in the 3MB-PP1–treated population compared with DMSO treated controls (Fig. 2 A). Deep sequencing revealed that the sgRNA distribution in 3MB-PP1–treated cells was significantly different compared with DMSO-treated cells (Fig. 2 B). The two highest-ranking genes in the screen were p53 and 53BP1 (false discovery rate <0.05; Fig. 2, C and D; and Fig. S1 E). Importantly, 53BP1 interacts directly with p53 but has not been previously implicated in the centrosome surveillance pathway (Iwabuchi et al., 1994; Joo et al., 2002).

To confirm 53BP1 as a novel hit, we repeated the CRISPR/Cas9 screen in SpCas9-expressing hTERT-RPE1 cells using the Plk4 inhibitor centrinone (Wong et al., 2015). p53 and 53BP1 emerged again as the top hits from this screen (false discovery rate <0.05; Fig. 2, E–G). To validate the role of 53BP1 in the centrosome surveillance pathway, we generated knockouts of p53 and 53BP1 in Plk4^{AS} cells. Inactivation of p53 or 53BP1 dramatically increased the clonogenic survival of Plk4^{AS} cells treated with 3MB-PP1 (Figs. 2 H and S1 F). Thus, our unbiased, genome-scale screening identified 53BP1 as a novel component of the centrosome surveillance pathway.

53BP1 is required to stabilize p53 after centrosome loss

Knockout of p53 did not alter the levels of 53BP1 and vice versa, showing these proteins are not required for one another's stability (Fig. 3, A and B). To test whether cells lacking 53BP1 lose centrosomes in the absence of Plk4 activity, we examined centriole number in p53 and 53BP1 knockout Plk4^{AS} cells over

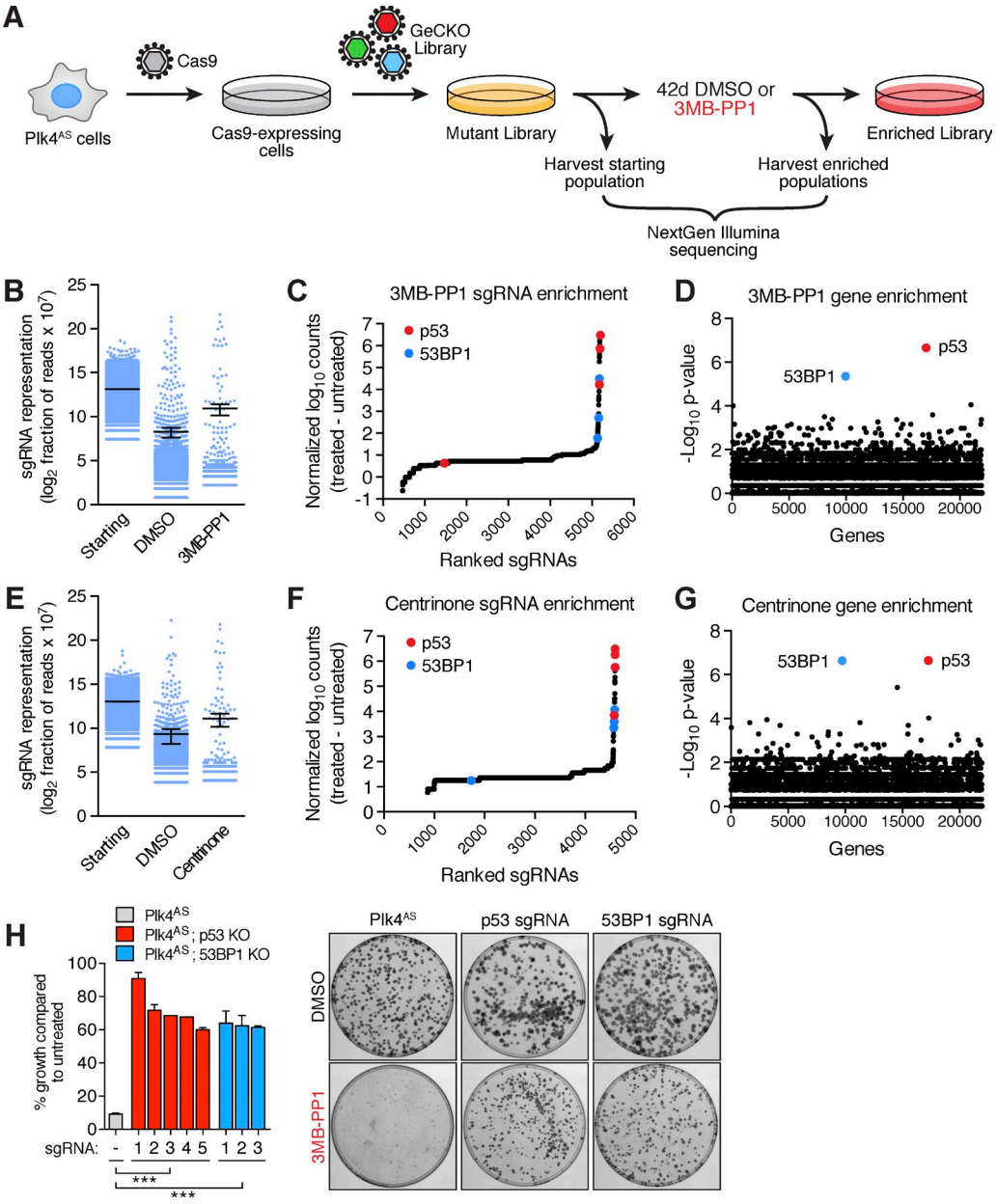

Figure 2. **A genome-wide CRISPR/Cas9 screen identifies 53BP1 and p53 as components of the centrosome surveillance pathway.** (A) Schematic of the pooled, positive selection CRISPR/Cas9 screen used to identify components of the centrosome surveillance pathway. (B) Graph showing the distribution of individual sgRNAs. Data are means ± SD. (C) Rank-ordered dot plot showing relative enrichment of individual sgRNAs after 3MB-PP1 treatment. (D) Identification of top candidate genes after 3MB-PP1 treatment using the MaGeCK ranking p-value analysis. (E) Graph showing the distribution of individual sgRNAs. Data are means ± SD. (F) Rank-ordered dot plot showing relative enrichment of individual sgRNAs after centrinone treatment. (G) Identification of top candidate genes after centrinone treatment using the MaGeCK ranking p-value analysis. (H) Graph showing the relative clonogenic growth of 3MB-PP1–treated Plk4^{AS} cells expressing individual sgRNAs. Data are means ± SEM (n = 2, performed in duplicate). Representative images of crystal violet–stained colonies. ***, $P \leq 0.001$.

the course of 1 week after Plk4 inhibition. Treatment of p53$^{-/-}$ or 53BP1$^{-/-}$ Plk4^{AS} cells with 3MB-PP1 led to a gradual reduction in centriole number as cells failed centriole duplication but continued to divide. 6 d after 3MB-PP1 treatment, >90% of p53 and 53BP1 knockout cells lacked centrioles (Fig. 3, C and D).

Centrosome loss increased total cellular and nuclear p53 levels (Fig. 3 E and Fig. S2 A). Importantly, knockout of 53BP1 prevented p53 stabilization in response to centrosome loss, suggesting that 53BP1 functions upstream of p53 in the centrosome surveillance pathway (Figs. 3 F and S2 A). Knockout of 53BP1 did not, however, prevent stabilization of p53 in response to doxorubicin-induced DNA damage (Fig. S2 A), showing that 53BP1 is not required for all p53-dependent responses.

USP28 functions together with 53BP1 to stabilize p53 after centrosome loss

We considered the possibility that during the selection period for the CRIPSR/Cas9 screen, sgRNAs that provide a modest growth advantage in cells lacking centrosomes may be outcompeted by the faster growth of cells containing sgRNAs targeting p53 or 53BP1. To investigate whether weaker hits may have been overlooked, we created knockouts for the top 40 ranked

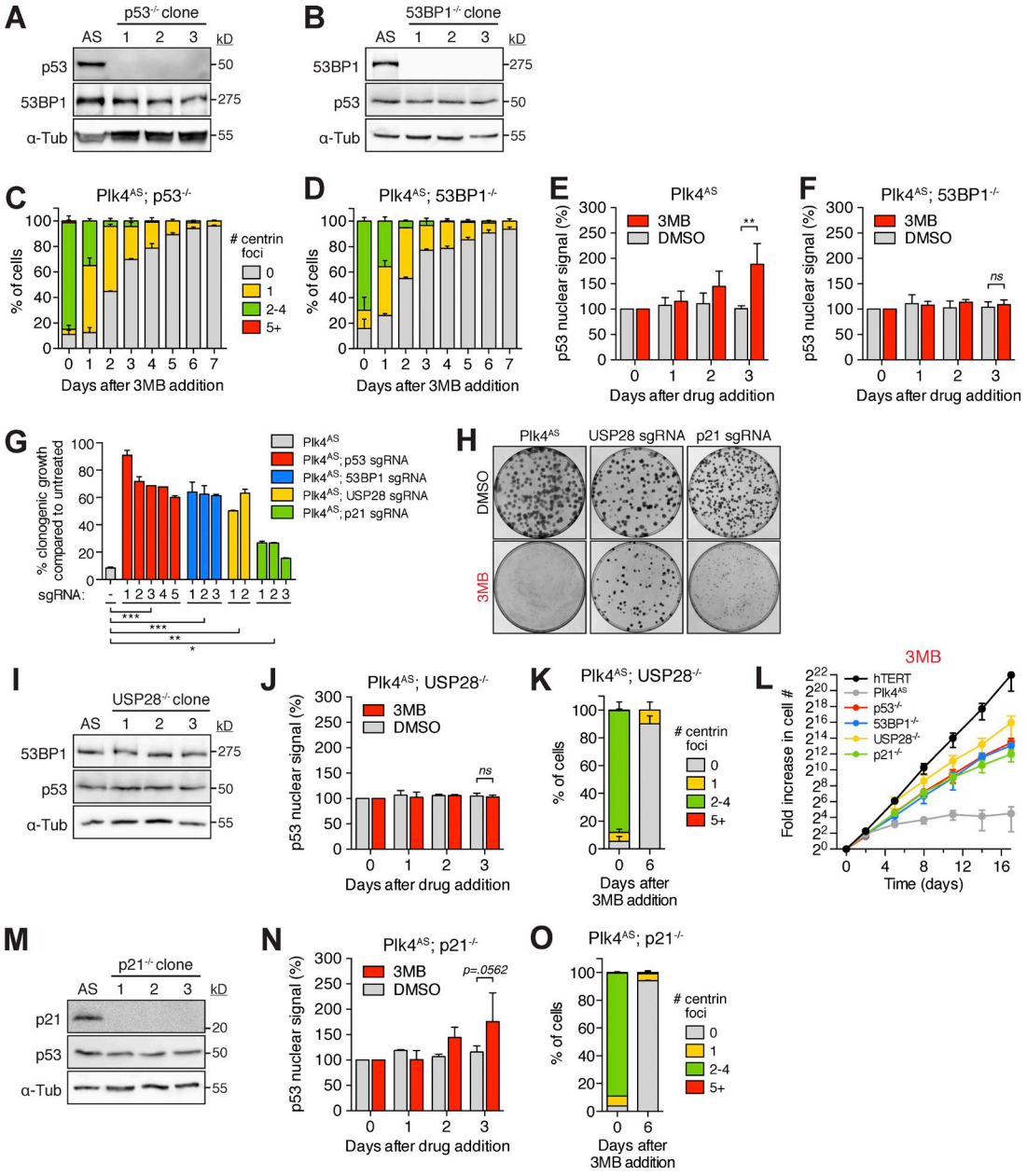

Figure 3. **p21 and USP28 are required for the centrosome surveillance pathway.** (A and B) Immunoblot showing the levels of p53 or 53BP1 in Plk4^{AS}; p53$^{-/-}$ and Plk4^{AS}; 53BP1$^{-/-}$ cells. (C and D) Centriole number distribution in interphase Plk4^{AS}; p53$^{-/-}$ and Plk4^{AS}; 53BP1$^{-/-}$ cells at times after addition of 3MB-PP1. Data are means ± SEM (n = 3, >80 cells per experiment). (E and F) Relative abundance of nuclear p53 in Plk4^{AS} and Plk4^{AS}; 53BP1$^{-/-}$ cells at times after addition of DMSO or 3MB-PP1. Data are means ± SEM (n = 3, >180 cells per experiment). (G) Relative clonogenic survival of 3MB-PP1–treated Plk4^{AS} cells expressing individual sgRNAs. Data are means ± SEM (n = 2, performed in duplicate). (H) Representative images of crystal violet stained colonies. (I) Immunoblot showing the level of p53 or 53BP1 protein in Plk4^{AS}; USP28$^{-/-}$ cells. (J) Relative abundance of nuclear p53 in Plk4^{AS}; USP28$^{-/-}$ cells at times after addition of DMSO or 3MB-PP1. Data are means ± SEM (n = 3, >180 cells per experiment). (K) Centriole number distribution in interphase Plk4^{AS}; USP28$^{-/-}$ cells at 6 d after addition of 3MB-PP1. Data are means ± SEM (n = 3, >80 cells per experiment). (L) Fold increase in cell number after 3MB-PP1 addition. Data are means ± SEM (n = 2, performed in triplicate). (M) Immunoblot showing the level of p21 or p53 in Plk4^{AS}; p21$^{-/-}$ cells. (N) Relative abundance of nuclear p53 in Plk4^{AS}; p21$^{-/-}$ cells at times after addition of DMSO or 3MB-PP1. Data are means ± SEM (n = 3, >180 cells per experiment). (O) Centriole number distribution in interphase Plk4^{AS}; p21$^{-/-}$ cells at 6 d after addition of 3MB-PP1. Data are means ± SEM (n = 3, >80 cells per experiment). ns (nonsignificant), P > 0.05; *, P ≤ 0.05; **, P ≤ 0.01; ***, P ≤ 0.001.

genes and analyzed the ability of each sgRNA to promote the growth of Plk4^{AS} cells in the presence of 3MB-PP1 (Fig. S1 E). Other than p53 and 53BP1, USP28 (ranked #29) was the only other sgRNA target that provided a significant growth advantage in Plk4^{AS} cells grown in 3MB-PP1 (Fig. 3, G and H; and Fig. S1, E and F). Importantly, USP28 is a deubiquitinating enzyme that has been shown to interact with 53BP1 (Zhang et al., 2006).

Knockout of USP28 did not alter basal levels of p53 or prevent p53 stabilization in response to doxorubicin-induced DNA damage (Fig. 3 I and Fig. S2, A and B). However, USP28$^{-/-}$ cells failed to stabilize p53 in response to centrosome loss (Figs. 3 J and S2 A). Cells lacking USP28 grew continually in the absence of Plk4 activity, and consequently, >90% of USP28 knockout cells lacked centrioles after 6 d of 3MB-PP1

treatment (Fig. 3, K and L; and Fig. S2 C). These data demonstrate that USP28 acts together with 53BP1 to stabilize p53 in response to centrosome loss.

To examine whether USP28 or 53BP1 knockout alters basal p53 stability, we examined p53 levels after cycloheximide addition in USP28$^{-/-}$ and 53BP1$^{-/-}$ cells. Loss of USP28 and 53BP1 did not alter basal p53 stability in Plk4^{AS} cells (Fig. S2 D). Furthermore, inhibiting p53 binding to MDM2 with Nutlin-3 elevated p53 levels to a similar extent in wild-type, USP28$^{-/-}$, and 53BP1$^{-/-}$ Plk4^{AS} cells (Fig. S2 E). We conclude that USP28 and 53BP1 do not alter p53 regulation by MDM2 or modulate basal p53 stability.

Inhibition of Plk4 kinase activity could have consequences in addition to prompting a failure of centriole duplication. We therefore tested whether loss of SAS6, a conserved structural component required for centriole assembly, also prevents cell growth and whether this can be overcome by inactivating components of the centrosome surveillance pathway (Dammermann et al., 2004; Leidel et al., 2005). Consistent with its essential role in cell growth, we were unable to generate SAS6 knockout clones in hTERT-RPE1 cells (Fig. S2 F). We did, however, identify multiple clones of USP28$^{-/-}$, 53BP1$^{-/-}$, and p53$^{-/-}$ cells that lacked SAS6 and centrosomes. These data suggest that centrosome loss, and not loss of Plk4 kinase activity per se, is responsible for activating the centrosome surveillance pathway.

p21 acts downstream of p53 in the centrosome surveillance pathway

The cyclin-dependent kinase inhibitor p21 (CDKN1A) is a transcriptional target of p53 that is responsible for promoting a p53-dependent G1 arrest in response to a variety of stress stimuli. Because p21 also emerged as a weak hit in the CRISPR/Cas9 screen (ranked #146; Fig. S1 E), we reasoned that p21 could contribute to the p53-dependent cell cycle arrest that occurs after centrosome loss. Indeed, p21 levels increased after Plk4 inhibition (Fig. S2 A). Knockout of p21 did not alter p53 abundance or prevent p53 stabilization after centrosome loss, consistent with p21 acting downstream of p53 (Fig. 3, M and N; and Fig. S2 A). p21 knockout increased the clonogenic survival of Plk4^{AS} cells in the presence of 3MB-PP1 (Fig. 3, G and H; and Fig. S1 F). In addition, p21$^{-/-}$ cells grew continually in the presence of 3MB-PP1, and by 6 d after 3MB-PP1 treatment, >90% of Plk4^{AS}; p21$^{-/-}$ cells lacked centrioles (Fig. 3, L and O; and Fig. S2 C).

The centrosome surveillance pathway is not activated by DNA damage

As USP28, 53BP1, and p53 have all been shown to play a role in the DNA damage signaling pathway, we asked whether cells that fail centrosome duplication acquire DNA damage. We first used immunoblotting to examine changes in the abundance of γ-H2AX. Although a brief treatment with doxorubicin increased γ-H2AX levels, no increase was observed in Plk4^{AS} cells treated with 3MB-PP1 (Fig. 4 A). In addition, doxorubicin-induced DNA damage led to robust phosphorylation of the ATM target sites p53 Ser15 and KAP1 Ser824, but phosphorylation of these sites was undetectable in Plk4^{AS} cells grown in the presence of 3MB-PP1 (Banin et al., 1998; Canman et al., 1998; White et al., 2006; Ziv et al., 2006; Fig. 4 A). We next examined 53BP1 foci formation using immunofluorescence microscopy. Although doxorubicin treatment led to a more than fourfold increase in the number of cells with more than five 53BP1 foci, no significant increase in foci formation was observed in Plk4^{AS} cells after centrosome duplication failure (Fig. 4 B). Collectively, our data offer no evidence for elevated DNA damage in cells that lose centrosomes.

Next, we tested whether proteins that function in the DNA damage pathway are required to arrest the cell cycle after centrosome loss. Chronic treatment with the ATM inhibitor KU-55933 did not prevent a cell cycle arrest after centrosome loss (Fig. S3, A and B). Additionally, ATM, RNF8, Chk1, and Chk2 are components of the DNA damage response, but knockout of these genes did not abolish the centrosome surveillance pathway (Fig. S1 E). Importantly, whereas Chk2$^{-/-}$ Plk4^{AS} cells did not proliferate in 3MB-PP1, loss of Chk2 attenuated DNA damage signaling and rescued cell growth in doxorubicin (Fig. 4, C–E). This suggests that the DNA damage response and centrosome surveillance are genetically separable pathways.

The E3 ubiquitin ligase RNF168 is required for the recruitment of 53BP1 to sites of DNA double-strand breaks (Doil et al., 2009; Mallette et al., 2012; Mallette and Richard, 2012). We created RNF168 knockout Plk4^{AS} cells and confirmed that although 53BP1 is present at normal levels in these cells, it fails to localize to sites of DNA damage (Fig. 4, F and G). Importantly, RNF168 knockout cells ceased proliferating after centrosome loss, demonstrating that localization of 53BP1 to sites of DNA damage is not required for it to function in the centrosome surveillance pathway (Fig. 4 H). These data suggest that 53BP1 plays a DNA damage–independent role in signaling through the centrosome surveillance pathway.

Finally, we tested the ability of cells lacking p53, 53BP1, or USP28 to proliferate after doxorubicin-induced DNA damage. As expected, treatment of Plk4^{AS} cells with doxorubicin dramatically reduced the fraction of cells that entered into S phase, as well as clonogenic survival (Figs. 4 I and S3 C). Although p53$^{-/-}$ cells progressed into S phase and formed colonies in the presence of doxorubicin, USP28$^{-/-}$ and 53BP1$^{-/-}$ cells did not. This demonstrates that the DNA damage response remains partly intact in cells lacking USP28 and 53BP1. Collectively, our evidence strongly indicates that DNA damage is not responsible for activating the centrosome surveillance pathway.

The cell cycle arrest induced by prolonged prometaphase requires the same signaling components as the centrosome surveillance pathway

To evaluate the effect of centrosome loss on mitotic duration, we grew p53$^{-/-}$, 53BP1$^{-/-}$, and USP28$^{-/-}$ Plk4^{AS} cells in 3MB-PP1 for 6 d and measured the length of mitosis in cells that lack centrosomes. Loss of centrosomes dramatically extended the duration of mitosis (mean of 153, 129, and 149 min in p53$^{-/-}$, 53BP1$^{-/-}$, and USP28$^{-/-}$ cells, respectively; Fig. 5 A). Previous work has shown that prolonging prometaphase to >90 min leads to p53-dependent arrest in RPE1 cells (Uetake and Sluder, 2010). This suggests that this mitotic timer may be dysfunctional in p53$^{-/-}$, 53BP1$^{-/-}$, and USP28$^{-/-}$ cells. To investigate this possibility, we first set out to determine the window of tolerance for prometaphase duration in the Plk4^{AS} RPE1 cells used in this study. Plk4^{AS} cells were treated with nocodazole for 6 h, and after drug washout, the proliferative fate of daughter cells monitored by time-lapse microscopy. Although 13% of daughters whose mothers spent <120 min in prometaphase failed to proliferate, prolonging the duration of prometaphase to >120 min caused a cell cycle arrest in 88% of the resulting daughters (Fig. 5 A). Although this response is not as robust

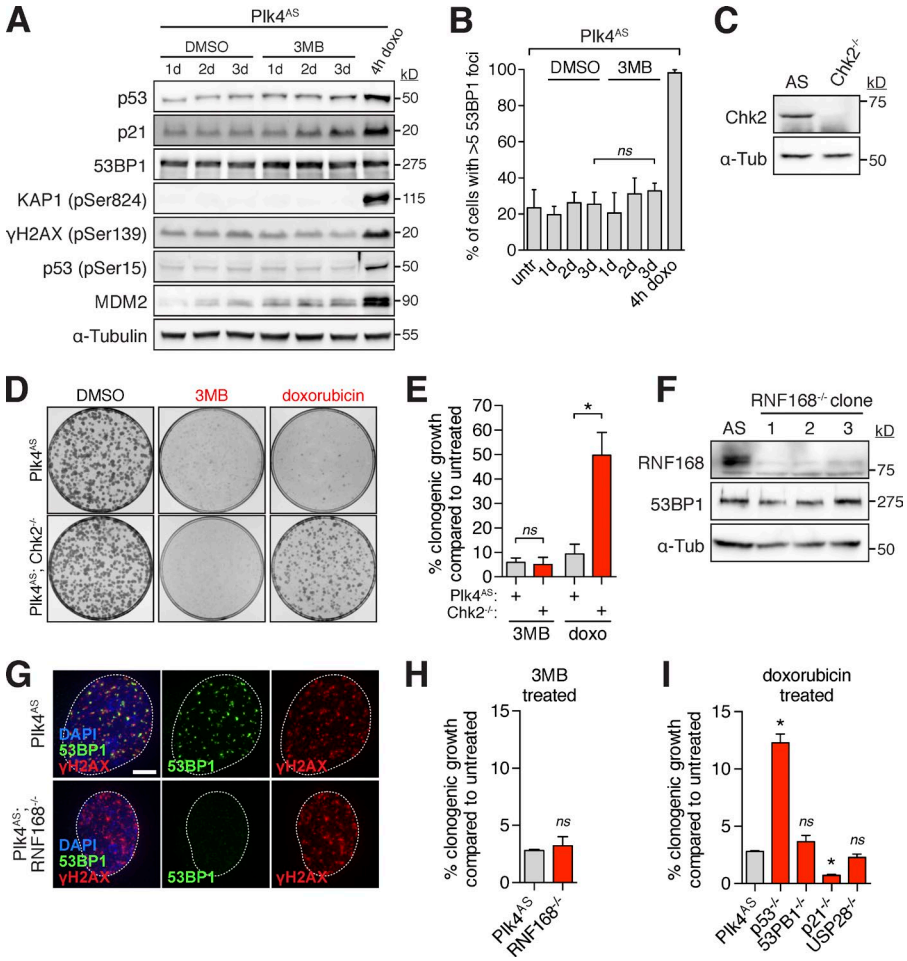

Figure 4. **The DNA damage response and centrosome surveillance pathway are genetically separable.** (A) Immunoblot showing the level of various proteins at 1, 2 or 3 d after addition of DMSO or 3MB-PP1. (B) Fraction of cells with more than five 53BP1 foci at times after addition of DMSO or 3MB-PP1. doxo, doxorubicin; untr, untreated. Data are means ± SEM (n = 3, >50 cells per experiment). (C) Immunoblot showing protein levels in Plk4^{AS}; Chk2$^{-/-}$ cells. (D) Representative images of crystal violet–stained colonies. (E) Relative clonogenic survival of 3MB-PP1 or 10 ng/ml doxorubicin–treated Plk4^{AS} cells. Data are means ± SEM (n = 3). (F) Immunoblot showing protein levels in Plk4^{AS}; RNF168$^{-/-}$ cells. (G) Images show the loss of 53BP1 foci formation in doxorubicin-treated Plk4^{AS}; RNF168$^{-/-}$ cells. Bar, 5 µm. (H) Graph shows the relative clonogenic survival of Plk4^{AS} and Plk4^{AS}; RNF168$^{-/-}$ cells treated with 3MB-PP1. Data are means ± SEM (n = 3). (I) Graph showing the relative clonogenic survival of 10 ng/ml doxorubicin-treated Plk4^{AS} cells. Data are means ± SEM (n = 3). ns (nonsignificant), P > 0.05; *, P ≤ 0.05.

as reported in unmodified hTERT-RPE1 cells, the mitotic timer is clearly functioning in Plk4^{AS} cells (Uetake and Sluder, 2010; Wong et al., 2015).

We next investigated whether the newly identified components of the centrosome surveillance pathway are also required to arrest cells after an increased mitotic duration. Consistent with previous work, nearly all p53$^{-/-}$ daughter cells proliferated regardless of the prometaphase duration in the preceding division (Fig. 5 B; Uetake and Sluder, 2010). Remarkably, knockout of USP28 and 53BP1 almost completely abolished the G1 arrest after a prolonged prometaphase. We conclude that the stresses generated by both centrosome loss and an extended prometaphase act through the same signaling components to stabilize p53 and cause a cell cycle arrest.

Because the centrosome surveillance pathway and the mitotic timer require the same components, we investigated whether activation of the mitotic timer could account for the cell cycle arrest that occurs in Plk4^{AS} cells after centrosome loss. To examine the effect of centrosome loss on cell division time, we monitored Plk4^{AS} cells by time-lapse microscopy at 1, 2, and 3 d after Plk4 inhibition. Untreated control cells progressed though mitosis with a mean time of 25 min (Fig. 5 C). Mitotic duration increased as cells progressed through successive divisions in the absence of Plk4 activity (mean of 40 min at 1 d, 60 min at 2 d, and 65 min at 3 d after 3MB-PP1 addition). Nevertheless, no mitosis exceeded a duration required to activate the mitotic timer (>120 min), suggesting that activation of the centrosome surveillance pathway cannot be simply explained by an increase in duration of a single division.

Distinct signal transduction cascades activate p53 in response to centrosome amplification or centrosome loss

We previously showed that Plk4 overexpression promotes centrosome amplification and a p53-dependent cell cycle arrest in hTERT-RPE1 cells (Holland et al., 2012). We therefore tested whether the proteins required to block proliferation after centrosome loss are also required to prevent cell growth in the presence of extra centrosomes. Although knockout of p53, and to a lesser extent p21, allowed for the growth of Plk4-overexpressing cells with supernumerary centrosomes, knockout of 53BP1 and USP28 did not (Fig. S3 D). A recent study showed that extra centrosomes trigger activation of the Hippo pathway kinase LATS2, which in turn stabilizes p53 (Ganem et al., 2014). However, knockout of LATS1 or LATS2 did not prevent growth arrest in cells after either centrosome loss or gain (Fig. S3, E and F). Collectively, these data suggest that distinct signaling pathways activate p53–p21 in response to centrosome loss or the presence of excess centrosomes (Fig. 5 D).

Our results reveal the existence of a USP28–53BP1–p53–p21 signaling axis that arrests cell cycle progression after centrosome loss. USP28 and p53 both bind to 53BP1 through the tandem C-terminal BRCT repeats (Joo et al., 2002; Knobel et al., 2014). We therefore speculate that 53BP1 could recruit USP28 to deubiquitinate and stabilize p53 in response to centrosome loss (Fig. 5 D). Although DNA breaks trigger p53 activation, several lines of evidence strongly suggest that DNA damage is not responsible for activating the centrosome surveillance pathway.

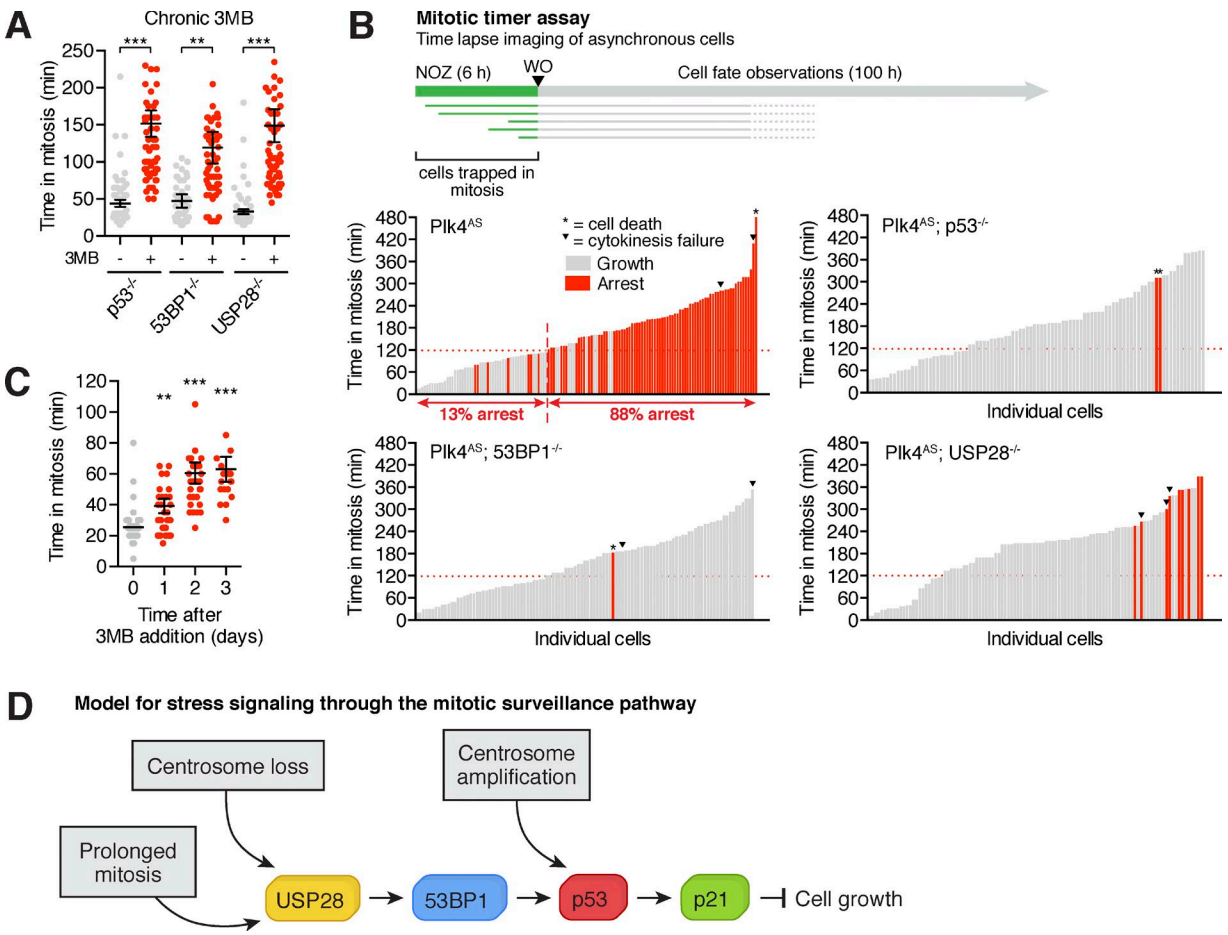

Figure 5. **Prolonged prometaphase and centrosome loss signal through the same components to arrest the cell cycle.** (A) Mitotic duration in histone H2B-EGFP–expressing p53$^{-/-}$, 53BP1$^{-/-}$, and USP28$^{-/-}$ Plk4^{AS} cells, grown in either DMSO or 3MB-PP1 for 6 d. Data are means ± SEM (n = 2, >25 cells per experiment). (B) Schematic of the mitotic timer experiment. Graph shows the prometaphase duration and proliferative capacity of 3MB-PP1–treated Plk4^{AS} cells. Each bar represents a daughter cell; its height represents the prometaphase duration of the mother cell, and its color represents the fate of the daughter. The dashed red line indicates the maximum time that mother cells spend in prometaphase before >85% of daughter cells undergo a cell cycle arrest. (C) Mitotic duration in histone H2B-EGFP–expressing Plk4^{AS} cells. Measurements were taken over a 24-h period at indicated times after 3MB-PP1 addition. Data are means ± SEM (n = 2, >25 cells per experiment). (D) A model for stress signaling inputs into the mitotic surveillance pathway. *, P ≤ 0.05; **, P ≤ 0.01; ***, P ≤ 0.001.

First, there is no detectable DNA damage in cells that fail centrosome duplication. Second, knockout of bona fide DNA damage components, including ATM, Chk1, Chk2, RNF8, and RNF168 do not prevent cell cycle arrest after centrosome loss. Third, preventing 53BP1 localization to sites of DNA damage prevents DNA damage-dependent functions of 53BP1, but it does not prevent growth arrest after a failure of centrosome duplication. Finally, although loss of USP28 or 53BP1 prevents activation of p53 in response to centrosome loss, their loss does not prevent p53 stabilization and cell cycle arrest in cells treated with the DNA damaging agent doxorubicin.

At present, the mechanism by which cells "sense" centrosome loss remains unclear. Although it is possible that the centrosome surveillance pathway directly monitors centrosome number, we feel this is unlikely for two reasons. First, p53, 53BP1, and USP28 do not localize to the centrosome in RPE1 cells (Fig. S3 G). Second, our evidence suggests that there are distinct pathways that activate p53 in cells with either too few or too many centrosomes, arguing against a common mechanism for detecting the wrong number of centrosomes. Therefore, we favor the interpretation that p53 activation is indirectly triggered by a stress associated with cell cycle progression after centrosome loss.

We have shown that, as well as being required for the centrosome surveillance pathway, USP28, 53BP1, and p53 are also required to prevent the growth of cells that delay in mitosis. This raises the possibility that the centrosome surveillance pathway is activated by a prolonged mitosis. Nevertheless, cells that fail centriole duplication delay in mitosis but do not exceed a mitotic duration in a single division that is sufficient to activate the mitotic timer (Lambrus et al., 2015; Wong et al., 2015). Because cells that fail centrosome duplication typically undergo three or four cell divisions before they cease proliferating, it is possible that the cumulative stress from successive delayed cell divisions eventually passes a threshold that triggers an arrest in cells failing centrosome duplication. Interestingly, 53BP1 localizes to unattached kinetochores in prometaphase, suggesting that it could play a signaling role during mitosis (Fig. S3 G; Jullien et al., 2002). Determining whether kinetochore localization of 53BP1 is required for the centrosome surveillance pathway and mitotic timer is an important area of future work.

Materials and methods

Cell culture

hTERT-RPE-1 cells were grown in DMEM:F12 medium (Cellgro; Corning) containing 10% fetal bovine serum (Sigma-Aldrich), 0.348% sodium bicarbonate, 100 U/ml penicillin, 100 U/ml streptomycin, and 2 mM L-glutamine. 293FT cells were grown in DMEM medium (Cellgro; Corning) containing 10% fetal bovine serum (Sigma-Aldrich), 100 U/ml penicillin, 100 U/ml streptomycin, and 2 mM L-glutamine. Cells were maintained at 37°C in a 5% CO_2 atmosphere with 21% oxygen. 3MB-PP1 (EMD Millipore) was dissolved in DMSO and used at a final concentration of 10 µM. Centrinone (a gift from K. Oegema, Ludwig Institute for Cancer Research, La Jolla, CA) was dissolved in DMSO and used at a final concentration of 125 nM. Cycloheximide (Sigma-Aldrich) was dissolved in water and used at a final concentration of 50 µg/ml. KU-55933 (Tocris Bioscience) was dissolved in DMSO and used at a final concentration of 10 µM. Nutlin-3 (Cayman Chemical) was dissolved in DMSO and used at a final concentration of 10 µM. Doxorubicin (Sigma-Aldrich) was dissolved in DMSO and used at a final concentration of 200 ng/ml unless otherwise stated.

Creation of Plk4^{AS} hTERT-RPE1 cells

To facilitate genome editing, we set out to knock out out the puromycin acetyltransferase (PAC) expressed in hTERT-RPE-1 cells. An sgRNA targeting PAC (5′-TGTCGAGCCCGACGCGCGTG-3′) was cloned into the px458 expression vector (48138; Addgene) that coexpresses the sgRNA from a U6 promoter and SpCas9-2A-GFP from a cytomegalovirus (CMV) promoter. Cells were transfected with the px458 plasmid and GFP-positive single cells isolated by FACS. Clones were split into duplicate wells, and one well received 3 µg/ml puromycin. A clone that showed complete cell death after 3 d of puromycin treatment was selected and used in all experiments described in this paper.

Plk4 gene targeting was performed in hTERT-RPE-1 cells using CRISPR/Cas9. In brief, a sgRNA targeting Plk4 (5′-AGATAG CAATTATGTGTATC-3′) was cloned into the px459 expression vector (48139; Addgene) that coexpresses the sgRNA from a U6 promoter and SpCas9-2A-puromycin from a CMV promoter. Cells were cotransfected with a 1:20 molar ratio of the px459 plasmid and a 160-bp single-stranded oligonucleotide repair template. The repair template introduced the L89G mutation, a silent AflIII restriction site, and a mutation in the SpCas9 protospacer-adjacent motif to prevent re-cutting after homology-directed repair. Transfected cells were selected for 3 d with 3 µg/ml puromycin, and single clones were isolated by limiting dilution. Genomic DNA was isolated from single clones and subjected to PCR using the following primers: forward, 5′-GCAGGAATGGTA CAGAGAGTCC-3′; reverse, 5′-GCAAAACTTTTATCCACCCAAA-3′. PCR products were digested with AflIII for 2 h. Clones with digested PCR products were sequenced to verify insertion of the L89G mutation. A single clone was identified that possessed the L89G mutation in one allele and a frameshift single-base-pair insertion in the second allele that led to the creation of a premature stop codon at amino acid 94 (L89G donor oligonucleotide: 5′-CTGAATTTTTGT ATATTTTAATTTATTATGCCCTTTCACATTTCAGCTTTATAACTA TTTTGAAGATAGCAATTACGTGTATCTAGTAGGAGAAATGTG CCATAATGGAGAAATGAACAGGTATCTAAAGAATAGAGTGAA ACCCTTCTCAGAAAATGAAG-3′).

Lentiviral production and transduction

The lentiCas9-Blasticidin (52962; Addgene), lentiGuide-Puromycin (52963; Addgene), or lentiGuide-Neomycin (this study) plasmid was cotransfected into 293FT cells with the lentiviral packaging plasmids psPAX2 and pMD2.G (12260 and 12259; Addgene). In brief, 8×10^6 293FT cells were seeded into a poly-L-Lysine–coated 15-cm culture dish the day before transfection. For each 15-cm dish, the following DNA was diluted in 1.2 ml OptiMEM (Thermo Fisher Scientific): 9 µg lentiviral vector, 12 µg psPAX2, and 3 µg pMD2.G. Separately, 72 µl of 1 µg/µl 25-kD polyethylenimine (Sigma-Aldrich) was diluted into 1.2 ml OptiMEM, briefly vortexed, and incubated at room temperature for 5 min. After incubation, the DNA and polyethylenimine mixtures were combined, briefly vortexed, and incubated at room temperature for 20 min. During this incubation, the culture media was replaced with 17 ml prewarmed DMEM + 1% FBS. The transfection mixture was then added drop-wise to the 15-cm dish. Viral particles were harvested 48 h after the media change and filtered through a 0.45-µm PVDF syringe filter. The filtered supernatant was either concentrated in 100 kD Amicon Ultra Centrifugal Filter Units (EMD Millipore) or used directly to infect cells. Aliquots were snap-frozen and stored at −80°C. For transduction, lentiviral particles were diluted in complete growth media supplemented with 10 µg/ml polybrene (Sigma-Aldrich) and added to cells.

CRISPR/Cas9 GeCKO screen

CRISPR/Cas9 pooled, knockout screens were performed essentially as described previously (Shalem et al., 2014; Chen et al., 2015). In brief, PAC knockout hTERT-RPE1 or Plk4^{AS} hTERT-RPE1 cells were transduced with the lentiCas9-blasticidin virus and single cells sorted into 96-well plates to isolate clonal cell lines. Multiple clones were screened by immunoblot for the FLAG epitope fused to the Cas9 protein. A SpCas9-hTERT-RPE1 and Plk4^{AS}-SpCas9-hTERT-RPE1 cell line with a high level of SpCas9 expression was selected for further use.

The human GeCKO v2 plasmid library was purchased from Addgene (1000000049) and plasmid DNA amplified according to the manufacturer's instructions. To produce virus, the GeCKO pooled plasmid library and the lentiviral packaging plasmids psPAX2 and pMD2.G were cotransfected into 40× 15-cm culture dishes of 293FT cells. Transfections were performed as described in the section above and viral particles were harvested, filtered, and concentrated. Aliquots were stored at −80°C.

Cells were transduced with the GeCKO library via spinfection. To find the optimal virus volumes for achieving an MOI ∼0.1, each new batch of virus was titered by spinfecting 3×10^6 cells with several different volumes of virus. In brief, 3×10^6 cells per well were seeded into a 12 well plate in growth media supplemented with 10 µg/ml polybrene. Each well received a different titrated virus amount (between 5 and 50 µl) along with a no-transduction control. The plate was centrifuged at 2,000 rpm for 2 h at room temperature. After the spin, media was aspirated and fresh growth media was added. The next day, cells were counted and each well was split into duplicate wells. One well received 3 µg/ml puromycin (Sigma-Aldrich) for 3 d. Cells were counted and the percent transduction calculated as the cell count from the replicate with puromycin divided by the cell count from the replicate without puromycin multiplied by 100. The virus volume yielding a MOI closest to 0.1 was chosen for large-scale transductions. A MOI of 0.1–0.2 corresponds to a single transduction percentage of 95% at 10% survival and 90% at 20% survival, respectively.

For the pooled screen a total of 12×10^7 SpCas9-hTERT-RPE1 or Plk4^{AS}-SpCas9-hTERT-RPE1 cells were infected at MOI ∼0.1 and selected with puromycin at 3 µg/ml for 3 d. MOI was calculated using a control well infected in parallel following the same procedure outlined in the paragraph above. Infected cells were expanded under puromycin selection for 7 d to allow editing to proceed to completion. After 7 d, 2×10^7 cells were spun down and frozen for genomic DNA extraction. In addition, 12×10^6 cells were seeded into each of two 15-cm culture dishes. One dish was treated with DMSO and the other with either centrinone

(SpCas9-hTERT-RPE1 cells) or 3MB-PP1 (Plk4^{AS}-SpCas9-hTERT-RPE1 cells). Cells were either passaged or fresh media was added every 3–4 d. Cell pellets with a minimum of 2×10^7 cells were taken at 42 d after drug addition at which point the screen was terminated.

Frozen cell pellets were thawed and genomic DNA was extracted with a GenElute Mammalian Genomic DNA extraction kit (Sigma-Aldrich). The sgRNA library for each sample was amplified and prepared for Illumina sequencing using a two-step PCR procedure, where the first PCR includes enough genomic DNA to preserve full library complexity and the second PCR adds appropriate sequencing adapters to the products from the first PCR. For the first PCR, a region containing the sgRNA cassette was amplified using primers specific to the sgRNA-expression vector (lentiGuide-PCR-F: 5′-AATGGACTATCATATGCTTACCGTAACTTGAAAGTATTTCG-3′; lentiGuide-PCR1-R: 5′-CTTTAGTTTGTATGTCTGTTGCTATTATGTCTACTATTCTTTCC-3′). The thermocycling parameters for the first PCR were 98°C for 30 s; 18–24 cycles of 98°C for 1 s, 62°C for 5 s, and 72°C for 35 s; and 72°C for 1 min. 1.5 µg DNA was used in each PCR reaction. Assuming 6.6 pg DNA per cell, ∼100× representation of the GeCKO library required ∼80 µg DNA per sample (54 PCR reactions). The resulting amplicons for each sample were pooled, gel purified, and used for amplification with barcoded second PCR primers. For each sample, we performed 14 reactions.

Primers for the second PCR include both a variable length sequence to increase library complexity and an 8-bp barcode for multiplexing of different biological samples (F2: 5′-AATGATACGGCGACCACCGAGATCTACACTCTTTCCCTACACGACGCTCTTCCGATCT-3′ [4–7-bp random nucleotides; 8-bp barcode], 5′-TCTTGTGGAAAGGACGAAACACCG-3′; R2: 5′-CAAGCAGAAGACGGCATACGAGATGTGACTGGAGTTCAGACGTGTGCTCTTCCGATCTTCTACTATTCTTTCCCCTGCACTGT-3′).

5 µl of the product from the first PCR reaction was used, and the thermocycling parameters for the second PCR were 98°C for 30 s and 18–24 cycles of 98°C for 1 s, 70°C for 5 s, 72°C for 35 s. Second PCR products were pooled, gel purified, and quantified using the Next Library Quantification kit (New England Biolabs, Inc.). Diluted libraries with 5% PhiX were sequenced with MiSeq (Illumina).

Sequencing data were processed for sgRNA representation using custom scripts. In brief, sequencing reads were first demultiplexed using the barcodes in the forward primer and then trimmed to leave only the 20 bp sgRNA sequences. The spacer sequences were then mapped to the spacers of the designed sgRNA library using Bowtie (Langmead et al., 2009). For mapping, a maximum of one mismatch was allowed in the 20-bp sgRNA sequence. Mapped sgRNA sequences were then quantified by counting the total number of reads. The total numbers of reads for all sgRNAs in each sample were normalized. Genes were ranked using the MaGeCK algorithm, which takes into account sgRNA enrichment as well as the number of sgRNAs targeting a particular gene (Li et al., 2014).

Antibody techniques

For immunoblot analyses, protein samples were separated by SDS-PAGE, transferred onto nitrocellulose membranes with a Trans-Blot Turbo Transfer System (Bio-Rad Laboratories) and then probed with the following antibodies: YL1/2 (rat anti–α-tubulin, 1:3,000; Pierce Antibodies), p53 (mouse, 1:1,000; EMD Millipore), 53BP1 (rabbit, 1:2,000; Novus Biologicals), MDM2 (mouse, 1:1,000; Thermo Fisher Scientific), Chk2 (mouse, 1:500; EMD Millipore), phospho-KAP1 (Ser824, rabbit, 1:1,000; Bethyl Laboratories, Inc.), p-histone H2A.X (Ser139; rabbit, 1:1,000; Cell Signaling Technology), phospho-p53 (Ser15, rabbit 1:1,000; Cell Signaling Technology), CDKN1A (rabbit, 1:1,000; NeoBioLab), RNF168 (rabbit, 1:1,000; EMD Millipore), LATS1 (rabbit, 1:1,000; Cell Signaling Technology), LATS2 (rabbit, 1:1,000; Cell Signaling Technology), and FLAG M2 (mouse, 1:1,000; Sigma-Aldrich).

For immunofluorescence, cells were grown on 18-mm glass coverslips and fixed for 10 min in either 4% formaldehyde at room temperature, or 100% ice cold methanol at −20°C for 10 min. Cells were blocked in 2.5% FBS, 200 mM glycine, and 0.1% Triton X-100 in PBS for 1 h. Antibody incubations were conducted in the blocking solution for 1 h. DNA was stained with DAPI and cells were mounted in ProLong Gold Antifade (Invitrogen). Staining was performed with the following primary antibodies: p53 (mouse, 1:1,000; EMD Millipore), 53BP1 (rabbit, 1:2,000; Novus Biologicals), 53BP1 (mouse, 1:1,000; EMD Millipore), USP28 (rabbit, 1:1,000; Proteintech), FLAG M2 (mouse, 1:1,000; Sigma-Aldrich), p-histone H2A.X (Ser139, rabbit, 1:1,000; Cell Signaling Technology), centrin (mouse, 1:1,000; EMD Millipore), CEP192-Cy5 (directly labeled goat, raised against CEP192 aa 1–211, 1:1,000; this study), and BUB1 (sheep, raised against BUB1 aa 336–489, 1:1,000; a gift from S. Taylor, the University of Manchester, Manchester, England, UK). Secondary donkey antibodies were conjugated to Alexa Fluor 488, 555, or 650 (Thermo Fisher Scientific).

For analysis of EdU incorporation, cells were pulsed with EdU for 12 h before fixation in 100% ice-cold methanol at −20°C for 10 min. Cells were washed three times with PBST and stained using a Click-It EdU Alexa Fluor 555 imaging kit (Thermo Fisher Scientific).

Immunofluorescence images were collected using a Deltavision Elite system (GE Healthcare) controlling a Scientific CMOS camera (pco.edge 5.5). Acquisition parameters were controlled by SoftWoRx suite (GE Healthcare). Images were collected at room temperature (25°C) using an Olympus 40× 1.35 NA, 60× 1.42 NA or Olympus, or 100× 1.4 NA oil objective at 0.2-µm z-sections. Images were acquired using Applied Precision immersion oil ($n = 1.516$). For quantitation of nuclear p53 signal intensity, 2D maximum intensity projections were saved as 16-bit TIFF images, and DAPI signal was used to threshold nuclei as regions of interest. For each nucleus, the integrated density of p53 signal was divided by nuclear area to give a signal/area value. Data were averaged over all cells in the panel and normalized to untreated population.

Live-cell microscopy

EGFP-tagged histone H2B was cloned into the FUGW backbone under the control of the CMV promoter and introduced into Plk4^{AS} cells using lentiviral delivery.

Histone H2B-EGFP–expressing Plk4^{AS} cells were seeded into four-chamber, 35-mm glass-bottom culture dishes (Greiner) and maintained at 37°C in an environmental control station. Images were collected using a Deltavision Elite system (GE Healthcare) controlling a Scientific CMOS camera (pco.edge 5.5.). Images were acquired with an Olympus 20× 0.75 NA air objective. Every 5 min, 7 × 3-µm z-sections were acquired in the FITC channel and by differential interference contrast. Movies were assembled and analyzed in FIJI. Mitotic duration was calculated as the time taken from nuclear envelope breakdown to mitotic exit.

Mitotic timer experiments tracing

For nocodazole treatment, coverslips were assembled into observation chambers with medium containing 0.08 µM nocodazole, and fields of cells were continuously followed by video time-lapse microscopy at 37°C for 6 h. After 6 h, the field of view was marked with a diamond scribe; the bottom of the observation chamber was removed and washed out with fresh medium several times before being reassembled with fresh medium as previously described (Uetake and Sluder, 2012). The previously marked fields were continuously followed for at least

96 h. Images were collected using a DMRXE microscope (Leica Biosystems) equipped with phase-contrast optics and a 10× 0.3 NA objective (Leica Biosystems). Images were captured with an Orca ER (Hamamatsu Photonics) camera using HCT software (Hamamatsu Photonics) and exported as AVI movies to be viewed with QuickTime (Apple).

Cell biology

To prepare cells for flow cytometry, cell pellets were fixed in cold 70% EtOH for 24 h, washed once in PBS, and resuspended in PBS supplemented with 10 µg/ml RNase A and 50 µg/ml propidium iodide. Samples were incubated at room temperature for 30 min and analyzed on a flow cytometer (FACSCalibur; BD). For clonogenic assays, 500 cells were seeded in a 10-cm^2 culture dish and left to grow for ∼10 d until colonies were visible by eye. Cells were fixed in methanol for 30 min at room temperature and colonies were stained with crystal violet (Sigma-Aldrich). Plates were imaged on a G:BOX Chemi XX6 (Syngene) and the fraction of the dish upon which growth occurred was determined using GeneSys software (Syngene). The percentage of clonogenic survival was calculated by dividing the area of growth in the presence of 3MB-PP1 by the area of growth of control DMSO-treated cells multiplied by 100.

Statistics

Differences were determined by one-tailed *t* test and are annotated as nonsignificant (ns; $P > 0.05$); *, $P \leq 0.05$; **, $P \leq 0.01$; and ***, $P \leq 0.001$.

Online supplemental material

Fig. S1 shows inhibition of Plk4 kinase activity activates the centrosome surveillance pathway and prevents cell growth. Fig. S2 shows USP28$^{-/-}$ and 53BP1$^{-/-}$ cells activate p53 in response to DNA damage, but not after centrosome loss. Fig. S3 shows knockout of 53BP1 or USP28 does not allow growth in cells overexpressing Plk4. Online supplemental material is available at http://www.jcb.org/cgi/content/full/jcb.201604054/DC1.

Acknowledgments

We thank Michelle Levine and Elizabeth Park for comments on this manuscript.

This work was supported by a March of Dimes Basil O'Connor Scholar Award, a Pew Scholar Award, a Kimmel Scholar Award, and National Institutes of Health research grants GM 114119 (A.J. Holland) and GM 30758 (G. Sluder).

The authors declare no competing financial interests.

Submitted: 13 April 2016
Accepted: 24 June 2016

References

Banin, S., L. Moyal, S. Shieh, Y. Taya, C.W. Anderson, L. Chessa, N.I. Smorodinsky, C. Prives, Y. Reiss, Y. Shiloh, and Y. Ziv. 1998. Enhanced phosphorylation of p53 by ATM in response to DNA damage. *Science.* 281:1674–1677. http://dx.doi.org/10.1126/science.281.5383.1674

Bazzi, H., and K.V. Anderson. 2014. Acentriolar mitosis activates a p53-dependent apoptosis pathway in the mouse embryo. *Proc. Natl. Acad. Sci. USA.* 111:E1491–E1500. http://dx.doi.org/10.1073/pnas.1400568111

Bettencourt-Dias, M., A. Rodrigues-Martins, L. Carpenter, M. Riparbelli, L. Lehmann, M.K. Gatt, N. Carmo, F. Balloux, G. Callaini, and D.M. Glover. 2005. SAK/PLK4 is required for centriole duplication and flagella development. *Curr. Biol.* 15:2199–2207. http://dx.doi.org/10.1016/j.cub.2005.11.042

Canman, C.E., D.S. Lim, K.A. Cimprich, Y. Taya, K. Tamai, K. Sakaguchi, E. Appella, M.B. Kastan, and J.D. Siliciano. 1998. Activation of the ATM kinase by ionizing radiation and phosphorylation of p53. *Science.* 281:1677–1679. http://dx.doi.org/10.1126/science.281.5383.1677

Chen, S., N.E. Sanjana, K. Zheng, O. Shalem, K. Lee, X. Shi, D.A. Scott, J. Song, J.Q. Pan, R. Weissleder, et al. 2015. Genome-wide CRISPR screen in a mouse model of tumor growth and metastasis. *Cell.* 160:1246–1260. http://dx.doi.org/10.1016/j.cell.2015.02.038

Conduit, P.T., A. Wainman, and J.W. Raff. 2015. Centrosome function and assembly in animal cells. *Nat. Rev. Mol. Cell Biol.* 16:611–624. http://dx.doi.org/10.1038/nrm4062

Dammermann, A., T. Müller-Reichert, L. Pelletier, B. Habermann, A. Desai, and K. Oegema. 2004. Centriole assembly requires both centriolar and pericentriolar material proteins. *Dev. Cell.* 7:815–829. http://dx.doi.org/10.1016/j.devcel.2004.10.015

Debec, A., W. Sullivan, and M. Bettencourt-Dias. 2010. Centrioles: active players or passengers during mitosis? *Cell. Mol. Life Sci.* 67:2173–2194. http://dx.doi.org/10.1007/s00018-010-0323-9

Doil, C., N. Mailand, S. Bekker-Jensen, P. Menard, D.H. Larsen, R. Pepperkok, J. Ellenberg, S. Panier, D. Durocher, J. Bartek, et al. 2009. RNF168 binds and amplifies ubiquitin conjugates on damaged chromosomes to allow accumulation of repair proteins. *Cell.* 136:435–446. http://dx.doi.org/10.1016/j.cell.2008.12.041

Ganem, N.J., S.A. Godinho, and D. Pellman. 2009. A mechanism linking extra centrosomes to chromosomal instability. *Nature.* 460:278–282. http://dx.doi.org/10.1038/nature08136

Ganem, N.J., H. Cornils, S.Y. Chiu, K.P. O'Rourke, J. Arnaud, D. Yimlamai, M. Théry, F.D. Camargo, and D. Pellman. 2014. Cytokinesis failure triggers hippo tumor suppressor pathway activation. *Cell.* 158:833–848. http://dx.doi.org/10.1016/j.cell.2014.06.029

Gönczy, P. 2012. Towards a molecular architecture of centriole assembly. *Nat. Rev. Mol. Cell Biol.* 13:425–435. http://dx.doi.org/10.1038/nrm3373

Habedanck, R., Y.D. Stierhof, C.J. Wilkinson, and E.A. Nigg. 2005. The Polo kinase Plk4 functions in centriole duplication. *Nat. Cell Biol.* 7:1140–1146. http://dx.doi.org/10.1038/ncb1320

Holland, A.J., W. Lan, S. Niessen, H. Hoover, and D.W. Cleveland. 2010. Polo-like kinase 4 kinase activity limits centrosome overduplication by autoregulating its own stability. *J. Cell Biol.* 188:191–198. http://dx.doi.org/10.1083/jcb.200911102

Holland, A.J., D. Fachinetti, Q. Zhu, M. Bauer, I.M. Verma, E.A. Nigg, and D.W. Cleveland. 2012. The autoregulated instability of Polo-like kinase 4 limits centrosome duplication to once per cell cycle. *Genes Dev.* 26:2684–2689. http://dx.doi.org/10.1101/gad.207027.112

Insolera, R., H. Bazzi, W. Shao, K.V. Anderson, and S.H. Shi. 2014. Cortical neurogenesis in the absence of centrioles. *Nat. Neurosci.* 17:1528–1535. http://dx.doi.org/10.1038/nn.3831

Iwabuchi, K., P.L. Bartel, B. Li, R. Marraccino, and S. Fields. 1994. Two cellular proteins that bind to wild-type but not mutant p53. *Proc. Natl. Acad. Sci. USA.* 91:6098–6102. http://dx.doi.org/10.1073/pnas.91.13.6098

Joo, W.S., P.D. Jeffrey, S.B. Cantor, M.S. Finnin, D.M. Livingston, and N.P. Pavletich. 2002. Structure of the 53BP1 BRCT region bound to p53 and its comparison to the Brca1 BRCT structure. *Genes Dev.* 16:583–593. http://dx.doi.org/10.1101/gad.959202

Jullien, D., P. Vagnarelli, W.C. Earnshaw, and Y. Adachi. 2002. Kinetochore localisation of the DNA damage response component 53BP1 during mitosis. *J. Cell Sci.* 115:71–79.

Khodjakov, A., and C.L. Rieder. 2001. Centrosomes enhance the fidelity of cytokinesis in vertebrates and are required for cell cycle progression. *J. Cell Biol.* 153:237–242. http://dx.doi.org/10.1083/jcb.153.1.237

Knobel, P.A., R. Belotserkovskaya, Y. Galanty, C.K. Schmidt, S.P. Jackson, and T.H. Stracker. 2014. USP28 is recruited to sites of DNA damage by the tandem BRCT domains of 53BP1 but plays a minor role in double-strand break metabolism. *Mol. Cell. Biol.* 34:2062–2074. http://dx.doi.org/10.1128/MCB.00197-14

Lambrus, B.G., Y. Uetake, K.M. Clutario, V. Daggubati, M. Snyder, G. Sluder, and A.J. Holland. 2015. p53 protects against genome instability following centriole duplication failure. *J. Cell Biol.* 210:63–77. http://dx.doi.org/10.1083/jcb.201502089

Langmead, B., C. Trapnell, M. Pop, and S.L. Salzberg. 2009. Ultrafast and memory-efficient alignment of short DNA sequences to the human genome. *Genome Biol.* 10:R25. http://dx.doi.org/10.1186/gb-2009-10-3-r25

Leidel, S., M. Delattre, L. Cerutti, K. Baumer, and P. Gönczy. 2005. SAS-6 defines a protein family required for centrosome duplication in *C. elegans* and in human cells. *Nat. Cell Biol.* 7:115–125. http://dx.doi.org/10.1038/ncb1220

Li, W., H. Xu, T. Xiao, L. Cong, M.I. Love, F. Zhang, R.A. Irizarry, J.S. Liu, M. Brown, and X.S. Liu. 2014. MAGeCK enables robust identification

of essential genes from genome-scale CRISPR/Cas9 knockout screens. *Genome Biol.* 15:554. http://dx.doi.org/10.1186/s13059-014-0554-4

Mallette, F.A., and S. Richard. 2012. K48-linked ubiquitination and protein degradation regulate 53BP1 recruitment at DNA damage sites. *Cell Res.* 22:1221–1223. http://dx.doi.org/10.1038/cr.2012.58

Mallette, F.A., F. Mattiroli, G. Cui, L.C. Young, M.J. Hendzel, G. Mer, T.K. Sixma, and S. Richard. 2012. RNF8- and RNF168-dependent degradation of KDM4A/JMJD2A triggers 53BP1 recruitment to DNA damage sites. *EMBO J.* 31:1865–1878. http://dx.doi.org/10.1038/emboj.2012.47

Moyer, T.C., K.M. Clutario, B.G. Lambrus, V. Daggubati, and A.J. Holland. 2015. Binding of STIL to Plk4 activates kinase activity to promote centriole assembly. *J. Cell Biol.* 209:863–878. http://dx.doi.org/10.1083/jcb.201502088

Shalem, O., N.E. Sanjana, E. Hartenian, X. Shi, D.A. Scott, T.S. Mikkelsen, D. Heckl, B.L. Ebert, D.E. Root, J.G. Doench, and F. Zhang. 2014. Genome-scale CRISPR-Cas9 knockout screening in human cells. *Science.* 343:84–87. http://dx.doi.org/10.1126/science.1247005

Silkworth, W.T., I.K. Nardi, L.M. Scholl, and D. Cimini. 2009. Multipolar spindle pole coalescence is a major source of kinetochore mis-attachment and chromosome mis-segregation in cancer cells. *PLoS One.* 4:e6564. http://dx.doi.org/10.1371/journal.pone.0006564

Sir, J.H., M. Pütz, O. Daly, C.G. Morrison, M. Dunning, J.V. Kilmartin, and F. Gergely. 2013. Loss of centrioles causes chromosomal instability in vertebrate somatic cells. *J. Cell Biol.* 203:747–756. http://dx.doi.org/10.1083/jcb.201309038

Tsou, M.F., and T. Stearns. 2006. Controlling centrosome number: licenses and blocks. *Curr. Opin. Cell Biol.* 18:74–78. http://dx.doi.org/10.1016/j.ceb.2005.12.008

Uetake, Y., and G. Sluder. 2010. Prolonged prometaphase blocks daughter cell proliferation despite normal completion of mitosis. *Curr. Biol.* 20:1666–1671. http://dx.doi.org/10.1016/j.cub.2010.08.018

Uetake, Y., and G. Sluder. 2012. Practical Methodology for Long-Term Recordings of Live Human Cells. Academic Press, New York. 43–52 pp.

White, D.E., D. Negorev, H. Peng, A.V. Ivanov, G.G. Maul, and F.J. Rauscher III. 2006. KAP1, a novel substrate for PIKK family members, colocalizes with numerous damage response factors at DNA lesions. *Cancer Res.* 66:11594–11599. http://dx.doi.org/10.1158/0008-5472.CAN-06-4138

Wong, Y.L., J.V. Anzola, R.L. Davis, M. Yoon, A. Motamedi, A. Kroll, C.P. Seo, J.E. Hsia, S.K. Kim, J.W. Mitchell, et al. 2015. Reversible centriole depletion with an inhibitor of Polo-like kinase 4. *Science.* 348:1155–1160. http://dx.doi.org/10.1126/science.aaa5111

Zhang, D., K. Zaugg, T.W. Mak, and S.J. Elledge. 2006. A role for the deubiquitinating enzyme USP28 in control of the DNA-damage response. *Cell.* 126:529–542. http://dx.doi.org/10.1016/j.cell.2006.06.039

Ziv, Y., D. Bielopolski, Y. Galanty, C. Lukas, Y. Taya, D.C. Schultz, J. Lukas, S. Bekker-Jensen, J. Bartek, and Y. Shiloh. 2006. Chromatin relaxation in response to DNA double-strand breaks is modulated by a novel ATM- and KAP-1 dependent pathway. *Nat. Cell Biol.* 8:870–876. http://dx.doi.org/10.1038/ncb1446